



Multi-modal Medical Image Fusion based on Two-scale Image Decomposition and Sparse Representation

Sarmad Maqsood, Umer Javed

Faculty of Engineering and Technology, IIU, Islamabad 44000, Pakistan



ARTICLE INFO

Article history:

Received 21 June 2019

Received in revised form 26 August 2019

Accepted 23 November 2019

Available online 9 December 2019

Keywords:

Image fusion

Multimodal medical image

contrast enhancement

sparse representation

ABSTRACT

Multimodality image fusion is the hot topic in medical imaging field which increases the clinical diagnosis accuracy through fusing complementary information of multimodality images. In this paper, a multimodal image fusion scheme is introduced based on two-scale image decomposition and sparse representation. In the proposed scheme, the source multimodal images are first processed through contrast enhancement technique so that the intensity distribution is improved for better visualization. A spatial gradient based edge detection technique is used for extracting the edge information from contrast stretched images. The enhanced multimodality images are then decomposed into two components: the base and detail layers. The final detail layer is extracted by using SSGSM. Finally, by using an enhanced decision maps and fusion scheme the fused image is obtained. The experimental results show that the proposed multimodal image fusion scheme outperforms with some others methods by performing qualitative and quantitative analysis.

© 2019 Elsevier Ltd. All rights reserved.

1. Introduction

Multi-modal medical image fusion combines the complementary information from different imaging modalities to acquire accurate information and enhance the quality of an image [1]. The fused image enhanced the visibility for human eyes and computer analysis. Medical image fusion methods are generally used in computer vision, clinical medicine, machine learning, digital imaging and pattern recognition with broad applications by fusing different methods of medical images [2].

Multi-modal image fusion provides diversified modalities like CT, MRI, SPECT, PET etc., for clinical diagnosis [2]. In the last few years large amount of image fusion schemes has been introduced to enhance the fusion performance. Image fusion have generally two main branches i.e., spatial-domain method and transform-domain method [3].

The spatial domain methods form the fuse image by choosing the pixels/regions/blocks of the source images without transformation [4]. This method further categorized into pixel based [3] and region based methods [5]. Transform domain techniques fuse the corresponding transform coefficients and apply inverse transformation to produce the fused image. Multi-scale transform (MST)

fusion technique is popular in multimodality image fusion. In transform domain method, a variety of transforms including the discrete wavelet transform based [6], dual tree complex wavelet transform based [7], contourlet transform based [8], curvelet transform based [9], non-subsampled contourlet transform based [10] and sparse representation based [11] techniques have been used in multimodality image fusion.

In recent times, Multiscale transform (MST) and Sparse representation (SR) based fusion methods have attracted great attention in transform domain methods and performed successfully in image recognition [12], image classification [13], image super-resolution [14], image feature extraction [15], image object identification [16] and multi-modality data fusion [17]. However, it is noticed that SR-based methods give improved performance than the MST-based methods. As a transform-based method, Li and Yang et al. [18] were the first to introduced the concept of image fusion with sparse representation. Li et al. [19] presented a de-noising approach for multimodal image fusion by group sparse representation, but, this scheme was not analyzed on color medical images. Nikolaos et al. [20] introduced a fusion framework for SR-based method in which the input images are classified into groups using the “sliding window” method, this approach shows a superior performance in capturing local salient features. Nejati et al. [21] and Yin et al. [22] presented a KSVD based multifocus image fusion method and produced better fusion results. Zhu et al. [17] presented a dictionary learning based image fusion technique, which improveded the

E-mail addresses: sarmad.maqsood001@gmail.com (S. Maqsood), umer.javed@iiu.edu.pk (U. Javed).

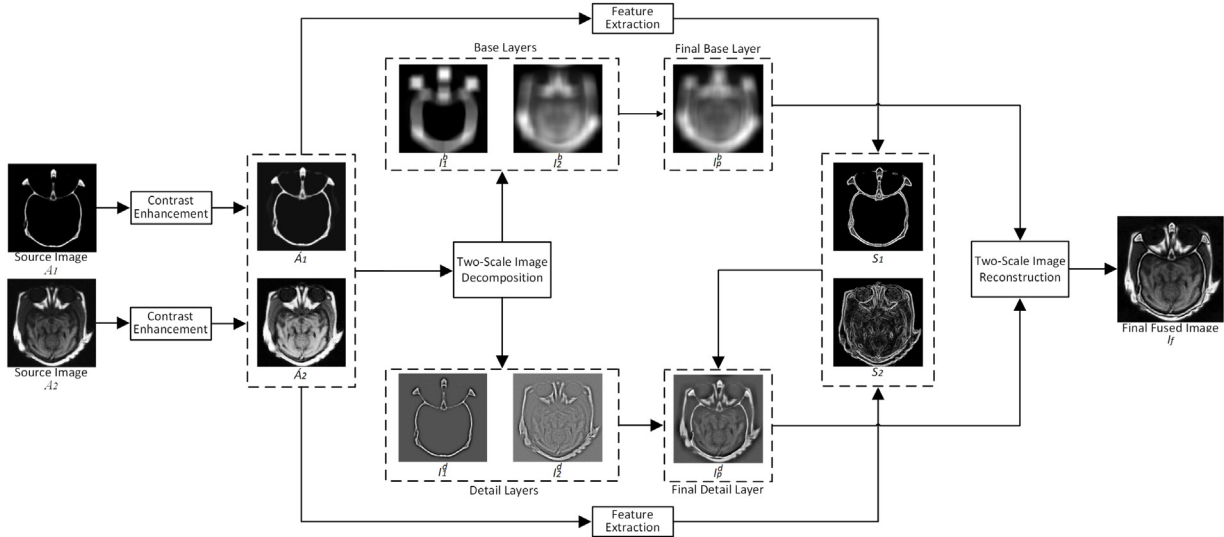


Fig. 1. Schematic diagram of proposed approach for image fusion algorithm.

performance of image details however, this scheme is not computationally effective because of the individual training for sub dictionaries and it is time consuming. Yin et al. [23] presented a image fusion technique based on joint sparsity model, smooth regions of this method leads to inaccurate segmentation and leads to poor visual effects. Li et al. [24] presented a relative application of different multi-scale transform based techniques and concludes that performance of NSCT-based scheme is superior to others methods.

However, SR and MST based fusion methods have achieved great performance, but, have some drawbacks in medical image fusion. The first drawback is the “max-L1” fusion rule may causes spatial difference in the multimodal medical fused images when the input images are taken by various imaging modalities [25]. Multi-scale transformation (MST) filter [25] applied to sparse representation based image fusion technique. Although, it has some limitations on decomposing certain types of images. The second drawback is the complex structure of input images that cannot be accurately represented by the trained dictionary [19]. For this drawback, Kim et al. [26] collected a training samples by k-means technique into some constructional groups and for each group particular sub-dictionary is trained that fits the specific structure. The complete dictionary has a strong representation ability. K-means technique is used to fix the numbers of cluster before clustering. In [27], Wang presented a multi-spectral image fusion for panchromatic images which can separately formed spatial and spectral dictionary. However, this method implemented only in visible and infrared image fusion.

In this paper, a new multlimodal image fusion method is proposed. This technique uses contrast stretching and spatial gradients to extract improved edges details from the source images. Two-scale image decomposition technique is used for image fusion algorithm. Finally, after processing the source images, decision maps and applying the fusion rule the fused image is formed. Proposed method produces better fusion results for multimodal image dataset than existing techniques.

The remaining paper is structured as follows. In section II the detailed procedure of proposed framework is explained. Section III describes the fusion metrics. Section IV includes experimental results and analysis and Section V concludes this paper.

2. Proposed multi-modality image fusion method

Let A_i be the source image having dimensions $M \times N$ where, $m = 1, 2, 3, \dots, M$, $n = 1, 2, 3, \dots, N$ and $i \in [1, 2]$ denotes CT and MRI images, respectively. Fig. 1 display the step procedure of proposed technique.

2.1. Pre-processing

Histogram equalization is most widely approach to enhance the low contrast images. The original image can be mapped as close as possible to the uniform distribution in the histogram equalization technique. Non-Parametric Modified Histogram Equalization (NMHE) [28], is incorporated as a pre-processing step to recover and preserve the average contrast of the original images A_i , i.e.,

$$\hat{A}_i \xleftarrow{\text{NMHE}[28]} A_i \quad (1)$$

NMHE is applied to source images to acquire the contrast enhanced images \hat{A}_i . Contrast enhancement leads to better intensity distribution and enhances the details in an image. The enhancement in edge information is shown in Fig. 2. The first row shows original source CT (Fig. 2(a)) and MRI (Fig. 2(b)) images, with their respective edge maps (Fig. 2(c, d)). The second row contains the contrast enhanced CT (Fig. 2(e)) and MRI (Fig. 2(f)) images with their gradient maps (Fig. 2(g, h)). It can be noted that there is a notable improvement in the edge information of contrast enhanced images as compared to original images.

2.2. Feature Extraction

Spatial Stimuli Gradient Sketch Model (SSGSM) [29], is used to obtain the edges map of each contrast enhanced images. The edge information in a fused image should have high contrast. This information is further used in computing the activity level maps which contain the focus information in all the images. The magnitude of the local stimuli is calculated by finding the local intensity in the perceived brightness at the spatial locations. The perceived brightness, C_i of a given image \hat{A}_i , is expressed as

$$C_i = \eta \log_{10}(\hat{A}_i) \quad (2)$$

where, \hat{A}_i denotes the source images and η represents the scaling factor.

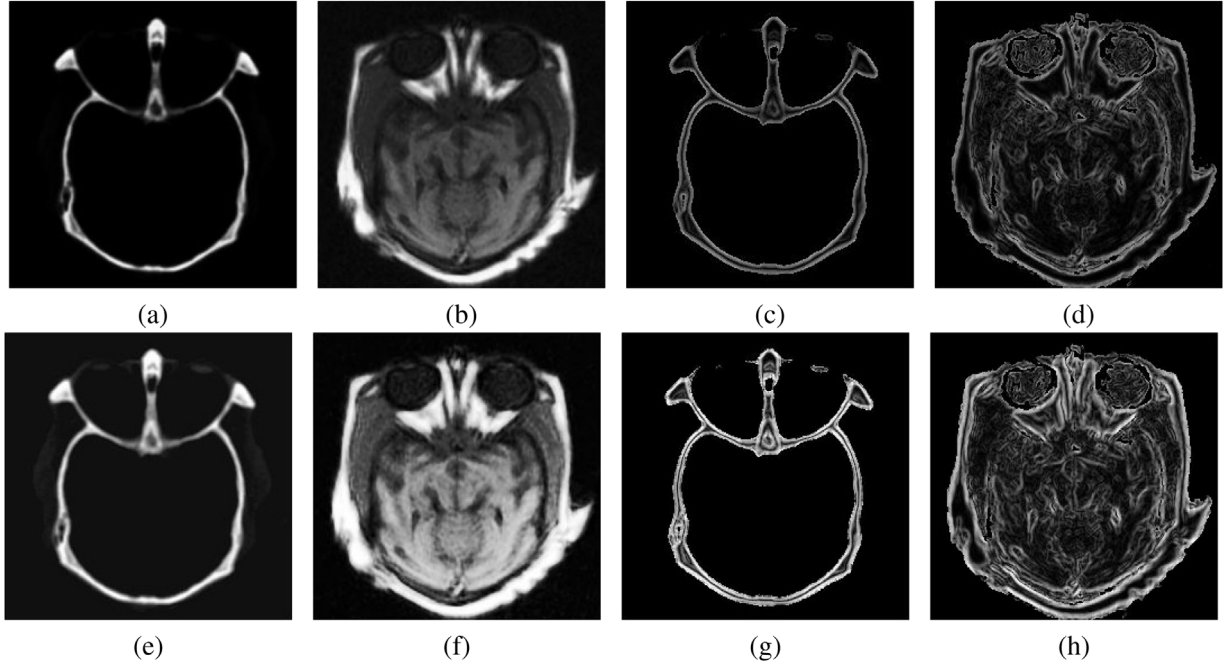


Fig. 2. The “CT and MRI” source images for contrast enhancement. (a,b) Source images, (c,d) Gradients of (a,b) obtained by SSGSM [29], (e,f) Contrast stretched using NMHE [28], (g,h) Gradients of (e,f) obtained by SSGSM [29].

Gradients represents the sharp intensity variations in the image. The gradient is a form of spatial distance measurement relative to the measured localized variability of the interpixel. The magnitude mathematically calculated as the net difference of the perceived brightness along m and n directions. The intensity variations of C_i along m (ξ_i^m) and n (ξ_i^n) axis are denoted by Z_i^m and Z_i^n . This can be formulated as,

$$[Z_i^m, Z_i^n]^{\text{gradient}} \leftarrow C_i \quad (3)$$

$$\xi_i^m = Z_i^m(e^{-|Z_i^m|}); \xi_i^n = Z_i^n(e^{-|Z_i^n|}) \quad (4)$$

The magnitude of local stimuli S_i can be calculated by,

$$S_i = \sqrt{(\xi_i^m)^2 + (\xi_i^n)^2} \quad (5)$$

2.3. Two-scale Image Decomposition

The image S_i then decomposed into base layers I_m^b having large scale variations and detail layers I_m^d having small scale variations. Base layer is achieved by solving the following problem.

$$I_m^b = \arg \min ||S_i - I_m^b||_F^2 + \delta(||h_x * I_m^b||_F^2 + ||h_y * I_m^b||_F^2) \quad (6)$$

where, $h_x = [-1 \ 1]$ is the horizontal gradient operator, $h_y = [-1 \ 1]^T$ is the vertical gradient operator and δ denotes the regularization parameter. The detail layer I_m^d is attained by subtraction.

$$I_m^d = S_i - I_m^b \quad (7)$$

2.4. Detail Layer Fusion

The sparse coefficient maps $S_{m,n}, n \in \{1, \dots, N\}$ of each detail layer I_m^d is achieved by solving the CSR model with approach in [30]:

$$S_{m,n} = \arg \min \frac{1}{2} \left(\sum_{n=1}^N k_m * S_{m,n} - I_m^d \right)_2^2 + \lambda \sum_{n=1}^N ||S_{m,n}||_1 \quad (8)$$

Let, $S_{m,1:N}(x, y)$ indicates content of $S_{m,n}$ at location (x, y) . The $S_{m,1:N}(x, y)$ is N dimensional vector. The technique utilized in SR

based image fusion method [11], the l_1 -norm of $S_{m,1:N}(x, y)$ is acquire as the activity level measure of the enhanced images. Therefore, the activity level map $\bar{P}_m(x, y)$ is achieved by

$$\bar{P}_m(x, y) = ||S_{m,1:N}(x, y)||_1 \quad (9)$$

Then, a final activity level map is obtained by applying window based averaging approach on $\bar{P}_m(x, y)$.

$$\bar{P}_m(x, y) = \frac{\sum_{k=-q}^q \sum_{l=-q}^q P_m(x+k, y+l)}{(2q+1)^2} \quad (10)$$

where, q determines the window size. With the larger value of q this technique is also robust to mis-registration, however, at the same time some minor details may be lost. A small scale detail usually exist in multimodal image fusion, therefore, it is more convenient to acquire a smaller q .

The fused coefficient maps are obtained by applying “choose-max” method.

$$S_{p,1:N}(x, y) = S_{m^*,1:N}(x, y), m^* = \arg \max(\bar{P}_m(x, y)) \quad (11)$$

Finally, the detail layers fusion result is reconstructed by

$$I_p^d(x, y) = \sum_{n=1}^N k_m * S_{p,n} \quad (12)$$

where, I_p^d is a final detail layer.

2.5. Base Layer Fusion

The averaging fusion rule is applied to multimodal image fusion to fuse the base layer.

$$I_p^b(x, y) = \frac{1}{M} \sum_{m=1}^M I_m^b(x, y) \quad (13)$$

where, I_p^b is a final base layer.

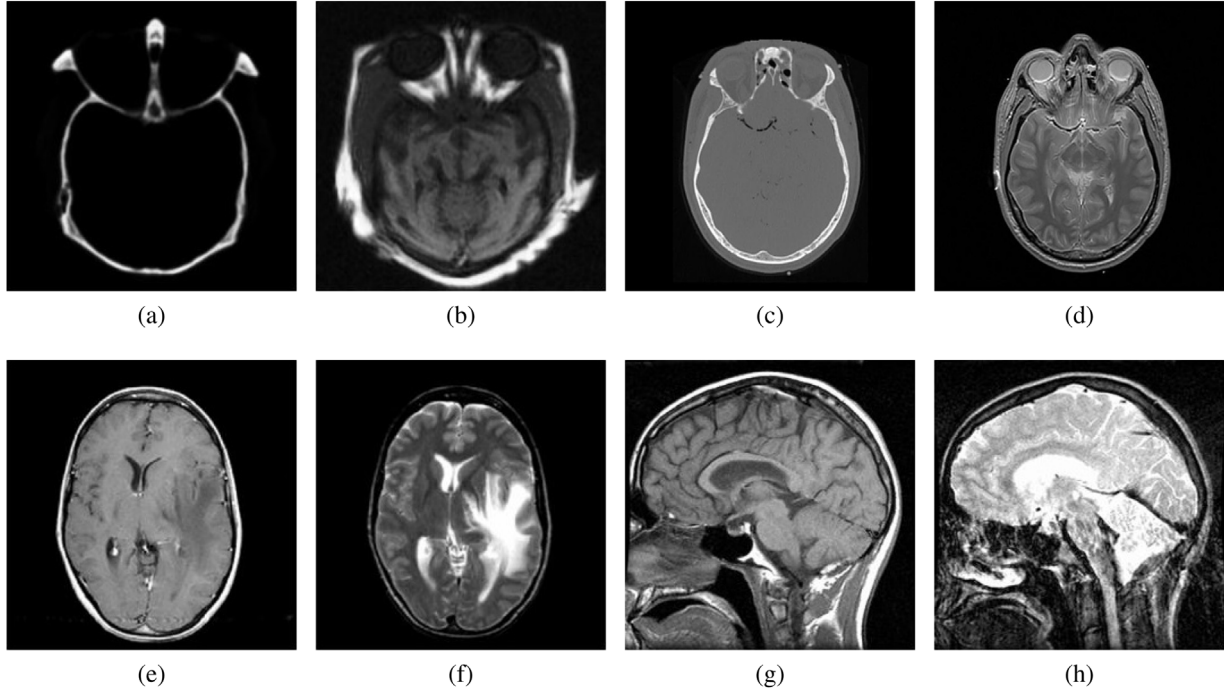


Fig. 3. The source images for multimodal image dataset: (a,b) Med-1, (c,d) Med-2, (e,f) Med-3 and (g,h) Med-4.

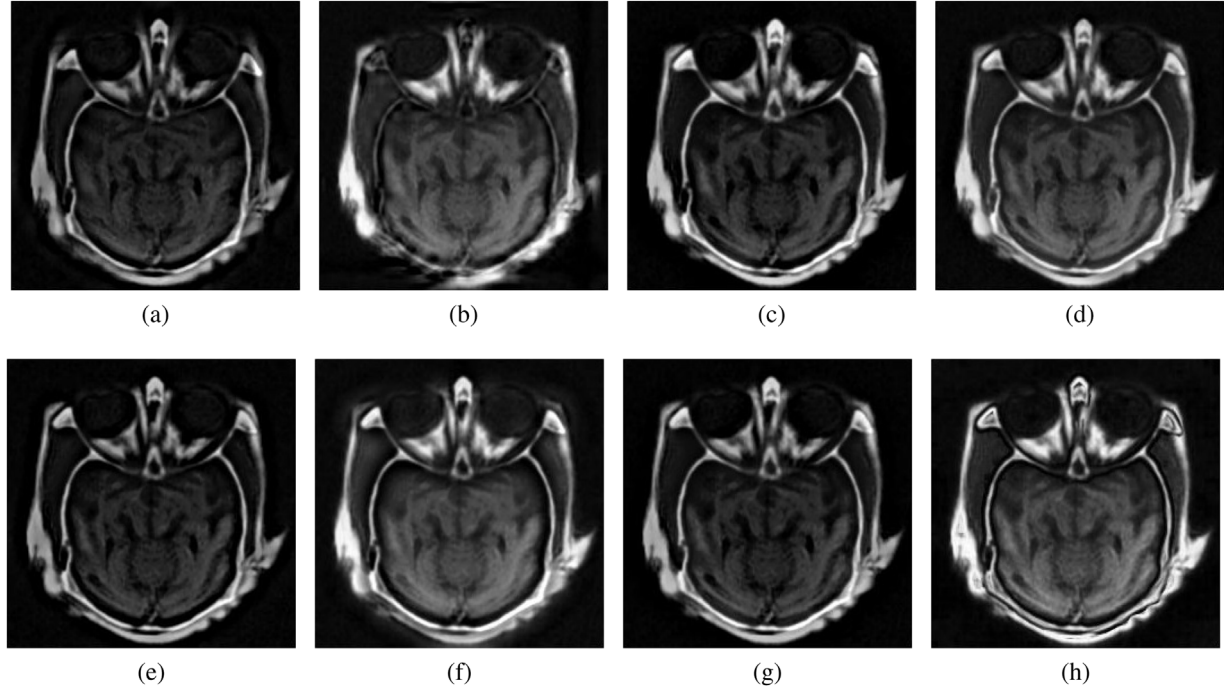


Fig. 4. The “Med-1” source image. (a)-(h) Fused images obtained using DTCWT [7], DWT [6], LP [35], GFF [36], NSCT [10], NSST-PAPCNN [37], CSMCA [38] and proposed method respectively.

2.6. Two-scale Image Reconstruction

The fused image $I_f(x, y)$ is formed by the linear integration of final fused detail layer $I_p^d(x, y)$ and fused base layer $I_p^b(x, y)$.

$$I_f(x, y) = I_p^d(x, y) + I_p^b(x, y) \quad (14)$$

Image fusion is used to overcome the limitation in a multi-modal imaging, enabling reconstruction and prediction of the missing information from MRI. The reconstruction of an image provides a

sharp, fresh image, and also resolve particular information at finer scales. The MRI along with other modalities when used together with image fusion method have shown to enhance the imaging accuracy, and practical clinical applicability.

3. Objective Evaluation Metrics

To evaluate the effectiveness of other image fusion schemes, some quantitative measurements are used to verify the perfor-

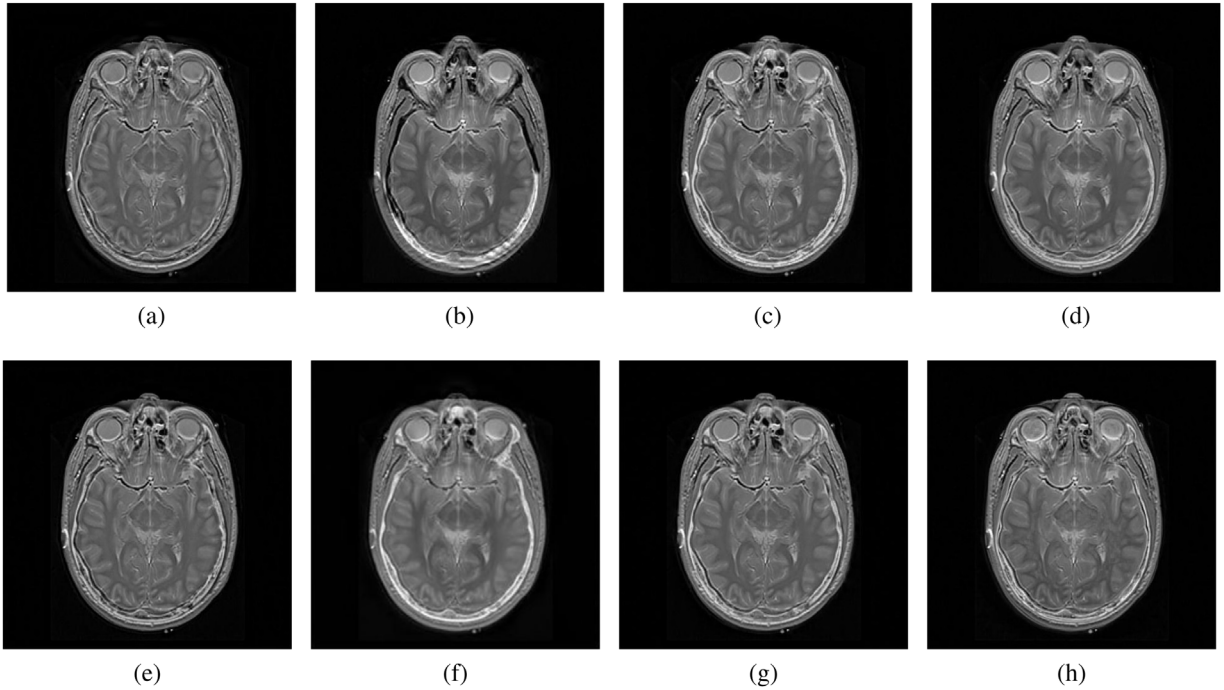


Fig. 5. The “Med-2” source image. (a)-(h) Fused images obtained using DTCWT [7], DWT [6], LP [35], GFF [36], NSCT [10], NSST-PAPCNN [37], CSMCA [38] and proposed method respectively.

mance. Five metrics are used for quantitatively evaluation, are Entropy (EN) [25], Spatial Structural Similarity (SSS) $Q^{AB/F}$ [31], Mutual Information (MI) [32], Feature Mutual Information (FMI) [33] and Visual Information Fidelity (VIF) [34] to check the perfection and superiority of the proposed multimodal image fusion method. For these metrics, the larger value usually shows a better result.

4. Experimental Results

4.1. Experimental setup

The proposed image fusion method is compared with some other latest algorithms to certify the effectiveness and superiority on multi-modal medical images. The datasets for multimodality image fusion acquired from [17]. The experiments are performed on a laptop in Matlab R2016b and on a Quad Core Intel(R) 2.4GHz processor with 4GB RAM. To determine the superiority of proposed method a comparison is performed with existing image fusion methods i.e., discrete wavelet transform (DWT) [6], dual tree complex wavelet transform (DTCWT) [7], laplacian pyramid (LP) [35], guided filtering based fusion (GFF) [36], non-subsampled contourlet transform (NSCT) [10], NSST-PAPCNN [37] and convolutional sparsity based morphological component analysis (CSMCA) [38]. The codes of all the above-mentioned methods are publicly available. The size of source images used are 256×256 .

4.2. Fusion results of medical images

Four pairs of multimodality medical images are used as displayed in Fig. 3. Using the state-of-the-art algorithms, the fusion results are illustrated in Figs. 4–7. The superiority of the fused image depends on both the visual observation and objective evaluation.

4.3. Visual observation of medical image fusion

Visual quality analysis of “Med-1” image dataset obtained by DTCWT, DWT, LP, GFF, NSCT, NSST-PAPCNN, CSMCA fusion

methods and the proposed scheme is displayed in Fig. 4(a)-(h) respectively. The source MRI image indicates soft tissues whereas CT image explains the bone structures and the hard tissues. For the better diagnosis, it is required to combine all the necessary information of these images into one fused image. The visual quality and contrast of the DTCWT (Fig. 4(a)) and DWT (Fig. 4(b)) fusion schemes are not up to mark. LP and CSMCA methods lost some particular information mostly in the overlapping parts of CT and MRI images and also containing some visual distortions in the fused image. Fusion result of GFF (Fig. 4(d)) and NSST-PAPCNN (Fig. 4(f)) are visually better than the remaining methods. However, the proposed multimodal image fusion method (Fig. 4(h)) provides superior visual quality of the edge details and the contrast than the other methods i.e., the soft tissues greatly discriminate from the bone structure.

Visual quality comparison of “Med-2” image dataset using numerous fusion schemes is displayed in Fig. 5. Source images of “Med-2” dataset is shown in (Fig. 3(c,d)). The fusion results of other methods DTCWT, DWT, LP, GFF, NSCT, NSST-PAPCNN and CSMCA are displayed in (Fig. 5(a)-(g)), respectively. Proposed image fusion scheme is presented in (Fig. 5(h)). From (Fig. 3(a,b,d)), DTCWT, DWT and GFF algorithms not integrated all the important information and may loss some complementary information when compared to source images. CSMCA method provides decent results as compared to other methods and integrated all necessary information and produce visually good image. However, the fusion result of proposed method provides visually more details when compared to NSST-PAPCNN and CSMCA methods. The proposed image fusion contrast is very pleasant as compared to other fusion methods.

Fusion results of “Med-3” image dataset using other fusion schemes and the proposed scheme are presented in Fig. 6. The DWT (Fig. 6(b)) and NSST-PAPCNN (Fig. 6(f)) results produced certain artifacts in the edge region. The GFF (Fig. 6(d)), NSCT (Fig. 6(e)) and CSMCA (Fig. 6(g)) methods gives better performance and fused image gives almost all the important information. However, in proposed method (Fig. 6(h)) the edges are well preserved and produced more details information in the fused image.

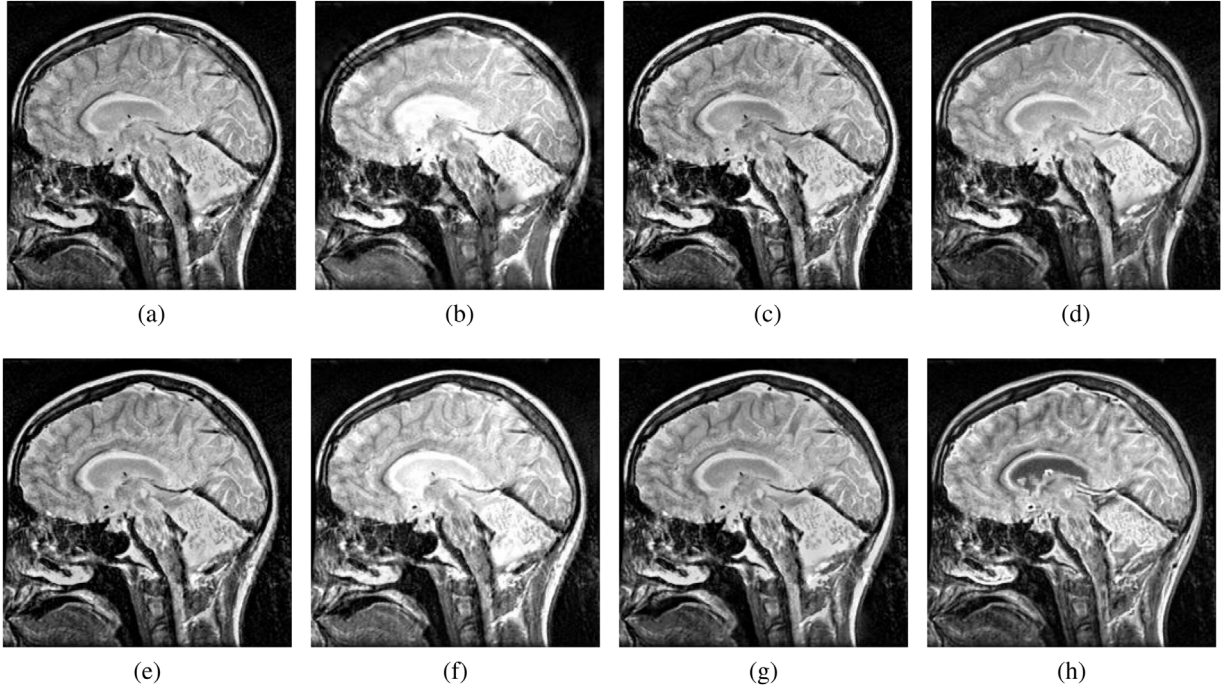


Fig. 6. The “Med-3” source image. (a)-(h) Fused images obtained using DTCWT [7], DWT [6], LP [35], GFF [36], NSCT [10], NSST-PAPCNN [37], CSMCA [38] and proposed method respectively.

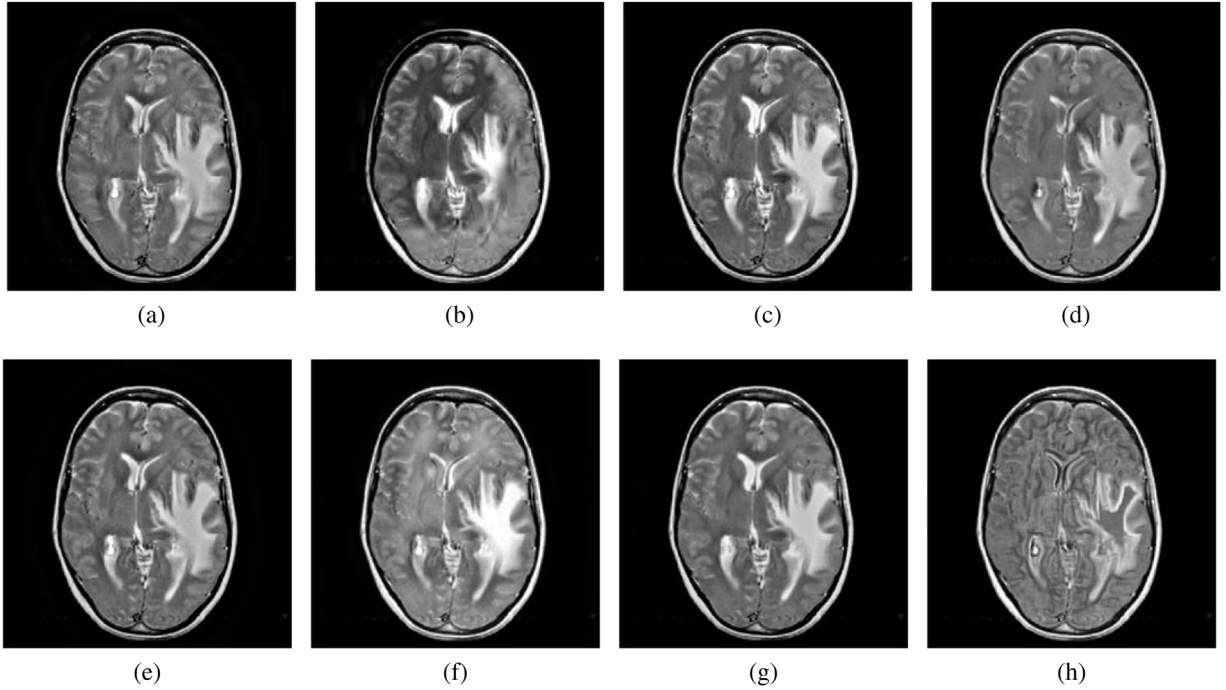


Fig. 7. The “Med-4” source image. (a)-(h) Fused images obtained using DTCWT [7], DWT [6], LP [35], GFF [36], NSCT [10], NSST-PAPCNN [37], CSMCA [38] and proposed method respectively.

Another fusion performance is verified on “Med-4” image dataset displayed in Fig. 7. Fused image of the proposed scheme is presented in (Fig. 7(h)) which greatly enhanced the edges and gives pleasant contrast than other fusion methods such as DTCWT, DWT, LP, GFF, NSCT, NSSTPAPCNN and CSMCA methods. Graphic representation of quantitative assessments of image datasets using different metrics are shown in Fig. 8(a)-(e).

After analyzing the quantitative assessment and visual quality of different schemes, it is concluded that the proposed method generates visually pleasant and high quality fusion result in majority of the cases and outperformed the existing fusion schemes for multimodal images. Table 1 shows that the proposed technique gives better assessment results than existing techniques.

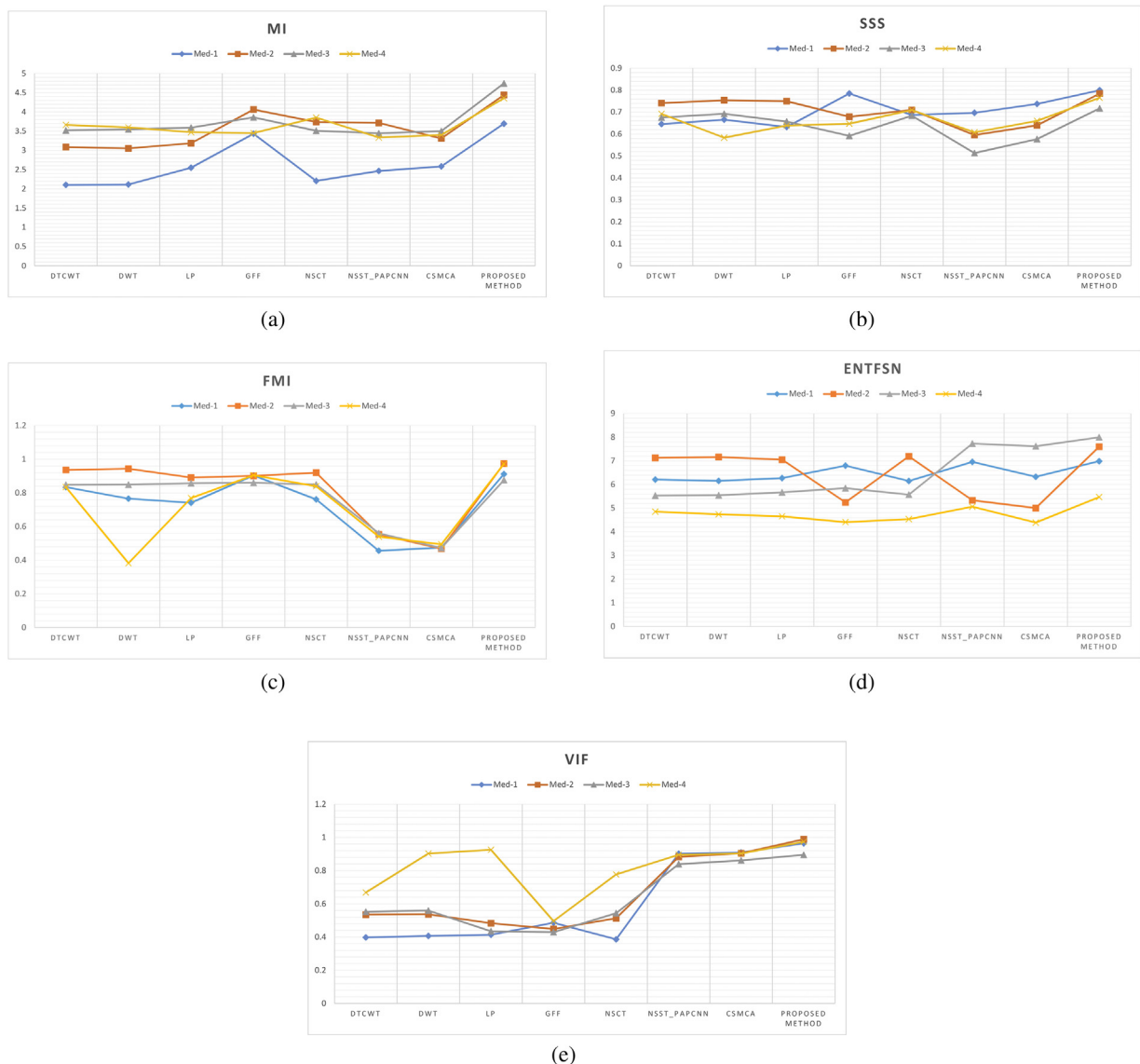


Fig. 8. Quantitative assessments comparison of image datasets using different metrics (a)MI [32] (b) $Q^{AB/F}$ [31] (c) $FMI_m^{x,y}$ [33] (d)EN [25] (e)VIF [34].

Table 1
The quantitative assessment results of different fusion methods.

Images	Fusion methods	MI [32]	$Q^{AB/F}$ [31]	$FMI_m^{x,y}$ [33]	EN [25]	VIF [34]
Med-1	DTCWT [7]	2.1044	0.6454	0.8341	6.2074	0.3976
	DWT [6]	2.1141	0.6656	0.7654	6.1512	0.4065
	LP [35]	2.5508	0.6321	0.7412	6.2724	0.4141
	GFF [36]	3.4313	0.7849	0.9032	6.7971	0.4864
	NSCT [10]	2.2087	0.6872	0.7612	6.1488	0.3864
	NSSTPAPCNN [37]	2.4665	0.6968	0.4559	6.9551	0.9015
Med-2	CSMCA [38]	2.5863	0.7373	0.4751	6.3274	0.9088
	Proposed	3.6949	0.7997	0.9116	6.9870	0.9645
	DTCWT [7]	3.0871	0.7414	0.9361	7.1287	0.5348
	DWT [6]	3.0523	0.7542	0.9438	7.1581	0.5369
	LP [35]	3.1847	0.7499	0.8914	7.0536	0.4832
	GFF [36]	4.0609	0.6788	0.9013	5.2463	0.4486
Med-3	NSCT [10]	3.7394	0.7101	0.9197	7.1873	0.5132
	NSSTPAPCNN [37]	3.7147	0.5956	0.5536	5.3329	0.8825
	CSMCA [38]	3.3098	0.6397	0.4679	5.0064	0.9048
	Proposed	4.4388	0.7842	0.9744	7.5970	0.9891
	DTCWT [7]	3.5201	0.6756	0.8479	5.5322	0.5521
	DWT [6]	3.5472	0.6922	0.8493	5.5481	0.5593
Med-4	LP [35]	3.5908	0.6571	0.8568	5.6692	0.4352
	GFF [36]	3.8595	0.5919	0.8596	5.8459	0.4295

Table 1 (Continued)

Images	Fusion methods	MI [32]	$Q^{AB/F}$ [31]	$FM_{m}^{x,y}$ [33]	EN [25]	VIF [34]
Med-4	NSCT [10]	3.5110	0.6837	0.8498	5.5703	0.5435
	NSSTPAPCNN [37]	3.4462	0.5136	0.5597	7.7278	0.8393
	CSMCA [38]	3.5008	0.5772	0.4728	7.6182	0.8615
	Proposed	4.7421	0.7169	0.8756	7.9945	0.8951
	DTCWT [7]	3.6632	0.6921	0.8339	4.8551	0.6679
	DWT [6]	3.5962	0.5835	0.3823	4.7393	0.9027
	LP [35]	3.4733	0.6391	0.7690	4.6547	0.9255
	GFF [36]	3.4514	0.6470	0.9047	4.4081	0.4961
	NSCT [10]	3.8544	0.7093	0.8395	4.5360	0.7769
	NSSTPAPCNN [37]	3.3372	0.6076	0.5401	5.0598	0.8960
	CSMCA [38]	3.4007	0.6601	0.4939	4.3896	0.9027
	Proposed	4.3580	0.7654	0.9721	5.4681	0.9737

5. Conclusion

A two-scale image decomposition and sparse representation based multimodality image fusion method is proposed. The source images are pre-processed using NMHE histogram equalization technique and their gradients are calculated using SSGSM. Further the images are decayed into two components (base layer and detail layer). Through which the more detail information and edge features can be transmitted into the fused image. Simulation results on various cases shows that the proposed image fusion scheme performed superior and provides better fusion performance both visually and quantitatively when compared to other fusion techniques. In future, the role of proposed algorithm will further be investigated for other image processing applications.

References

- [1] H. Li, Z. Yu, C. Mao, Fractional differential and variational method for image fusion and super-resolution, Neurocomputing 171 (2016) 138–148.
- [2] A.P. James, B.V. Dasarathy, Medical image fusion: A survey of the state of the art, Information Fusion 19 (2014) 4–19.
- [3] S. Li, X. Kang, L. Fang, J. Hu, H. Yin, Pixel-level image fusion: A survey of the state of the art, Information Fusion 33 (2017) 100–112.
- [4] H. Li, H. Qiu, Z. Yu, B. Li, Multifocus image fusion via fixed window technique of multiscale images and non-local means filtering, Signal Processing 138 (2017) 71–85.
- [5] M. Zribi, Non-parametric and region-based image fusion with Bootstrap sampling, Information Fusion 11 (2) (2010) 85–94.
- [6] Y. Yang, A novel DWT based multi-focus image fusion method, Procedia Engineering 24 (1) (2011) 177–181.
- [7] B. Yu, B. Jia, L. Ding, Z. Cai, Q. Wu, Hybrid dual-tree complex wavelet transform and support vector machine for digital multi-focus image fusion, Neurocomputing 182 (2016) 1–9.
- [8] S. Yang, M. Wang, L. Jiao, R. Wu, Z. Wang, Image fusion based on a new contourlet packet, Information Fusion 11 (2) (2010) 78–84.
- [9] F. Nencini, A. Garzelli, S. Baronti, L. Alparone, Remote sensing image fusion using the curvelet transform, Information Fusion 8 (2) (2007) 143–156.
- [10] H. Li, H. Qiu, Z. Yu, Y. Zhang, Infrared and visible image fusion scheme based on NSCT and low-level visual features, Infrared Physics and Technology 76 (2016) 174–184.
- [11] B. Yang, S. Li, Multifocus image fusion and restoration with sparse representation, IEEE Transactions on Instrumentation and Measurement 59 (4) (2010) 884–892.
- [12] H. Liu, Y. Yu, F. Sun, J. Gu, Visualtactile fusion for object recognition, IEEE Transaction on Automation Science and Engineering 14 (2) (2017) 996–1008.
- [13] J. Cao, J. Hao, X. Lai, C.M. Vong, M. Luo, Ensemble extreme learning machine and sparse representation classification, Journal of The Franklin Institute 353 (17) (2016) 4526–4541.
- [14] J. Yang, Z. Wang, Z. Lin, S. Cohen, T.S. Huang, Coupled dictionary training for image super-resolution, IEEE Transaction on Image Processing 21 (8) (2012) 3467–3478.
- [15] H. Liu, Y. Liu, F. Sun, Robust exemplar extraction using structured sparse coding, IEEE Transaction on Neural Network and Learning System 26 (8) (2015) 1816–1821.
- [16] H. Liu, D. Guo, F. Sun, Object recognition using tactile measurements: kernel sparse coding methods, IEEE Transaction on Instrument and Measurement 65 (3) (2016) 656–665.
- [17] Z. Zhu, Y. Chai, H. Yin, Y. Li, Z. Liu, A novel dictionary learning approach for multi-modality medical image fusion, Neurocomputing 214 (2016) 471–482.
- [18] B. Yang, S. Li, Multifocus image fusion and restoration with sparse representation, IEEE Transaction on Instrument and Measurement 59 (4) (2010) 884–892.
- [19] S. Li, H. Yin, L. Fang, Group-sparse representation with dictionary learning for medical image denoising and fusion, IEEE Transaction on Biomedical Engineering 59 (12) (2012) 3450–3459.
- [20] N. Mitianoudis, T. Stathaki, Pixel-based and region-based image fusion schemes using ICA bases, Information Fusion 8 (2) (2007) 131–142.
- [21] M. Nejati, S. Samavi, S. Shirani, Multi-focus image fusion using dictionary-based sparse representation, Information Fusion 25 (2015) 72–84.
- [22] H. Yin, Y. Li, Y. Chai, Z. Liu, Z. Zhu, A novel sparse representation-based multi-focus image fusion approach, Neurocomputing 216 (2016) 216–229.
- [23] H. Yin, S. Li, Multimodal image fusion with joint sparsity model, Optical Engineering 50 (6) (2011) 067007.
- [24] S. Li, B. Yang, J. Hu, Performance comparison of different multi-resolution transforms for image fusion, Information Fusion 12 (2) (2011) 74–84.
- [25] Y. Liu, S. Liu, Z. Wang, A general framework for image fusion based on multi-scale transform and sparse representation, Information Fusion 24 (2015) 147–164.
- [26] M. Kim, D.K. Han, H. Ko, Joint patch clustering-based dictionary learning for multimodal image fusion, Information Fusion 27 (2016) 198–214.
- [27] W. Wang, L. Jiao, S. Yang, Fusion of multispectral and panchromatic images via sparse representation and local auto regressive model, Information Fusion 20 (2014) 73–87.
- [28] S. Poddar, S. Tewary, D. Sharma, V. Karar, A. Ghosh, S.K. Pal, Non-parametric modified histogram equalisation for contrast enhancement, IET Image Processing 7 (2013) 641–652.
- [29] J.J. Mathew, A.P. James, Spatial stimuli gradient sketch model, IEEE Signal Processing Letters 22 (2015) 1336–1339.
- [30] B. Wohlberg, Efficient algorithms for convolutional sparse representation, IEEE Transcation on Image Processing 25 (1) (2016) 215–301.
- [31] V.S. Petrović, C.S. Xydeas, Sensor noise effects on signal-level image fusion performance, Information Fusion 4 (2003) 167–183.
- [32] M. Hosny, S. Nahavandi, D. Vreighton, Comments on information measure for performance of image fusion, Electronics Letters 44 (18) (2008) 1066–1067.
- [33] M.B.A. Haghighat, A. Aghagolzadeh, H. Seyedarabi, A non-reference image fusion metric based on mutual information of image features, Computers and Electrical Engineering 37 (2011) 744–756.
- [34] Y. Han, Y. Cai, Y. Cao, X. Xu, A new image fusion performance metric based on visual information fidelity, Information Fusion 14 (2) (2013) 127–135.
- [35] J. Du, W. Li, B. Xiao, Union laplacian pyramid with multiple features for medical image fusion, Neurocomputing 194 (19) (2016) 326–339.
- [36] S. Li, X. Kang, J. Hu, Image fusion with guided filtering, IEEE Transactions on Image Processing 22 (7) (2013) 2864–2875.
- [37] M. Yin, X. Liu, Y. Liu, X. Chen, Medical Image Fusion With Parameter-Adaptive Pulse Coupled-Neural Network in Nonsubsampled Shearlet Transform Domain, IEEE Transactions on Instrumentation and Measurement 68 (1) (2019) 49–64.
- [38] Y. Liu, X. Chen, R.K. Ward, Z.J. Wang, Medical Image Fusion via Convolutional Sparsity Based Morphological Component Analysis, IEEE Signal Processing Letters 26 (3) (2019) 485–489.